University of Utah, 1988.
5. W. R. Gombotz, A. S. Hoffman, J. M. Harris, B. Hovanes, G. H. Wang, and A. Safranj, "IUPAC Macromolecules Symposium", Seoul, Korea, June, 1989.
6. P. G. de Gennes, *Ann. Chim.*, **77**, 389 (1987).
7. H. J. Taunton, C. Toprakcioglu, L. J. Fetters, and J. Klein, *Nature (London)*, **332**, 712 (1988).
8. J. Klein and P. Luckham, *Nature (London)*, **300**, 429 (1982).
9. J. Klein and P. Luckham, *Macromolecules*, **17**, 1041 (1984).
10. P. Luckham and J. Klein, *Macromolecules*, **18**, 721 (1985).
11. J. N. Israelachvili and G. J. Adams, *J. Chem. Soc., Faraday Trans. 1*, **79**, 975 (1978).
12. S. J. Alexander, *J. Phys. (Les Ulis, Fr.)*, **38**, 983 (1977).
13. P. G. de Gennes, *Acad. Sci. Paris*, **300**, 839 (1985).
14. S. Patel, M. Tirrell, and G. Hadziioannou, *Colloids Surf.*, **31**, 157 (1988).
15. P. F. Luckham and J. Klein, *J. Chem. Soc. Faraday Trans.*, **86**, 1363 (1990).
16. J. Klein and P. F. Luckham, *Macromolecules*, **19**, 2007 (1986).
17. H. J. Taunton, C. Toprakciglu, and J. Klein, *Macromolecules*, **21**, 3333 (1988).
18. H. J. Taunton, C. Topracioglu, L. J. Fetters, and J. Klein, *ACS: Div. of Polym. Chem. (Polym. Preprints)*, **30**, 368 (1989).
19. H. Tadokoro, Y. Chatani, T. Yoshihara, S. Tahara, and M. Murahashi, *Makromol. Chem.*, **73**, 109 (1964).
20. Y. Takahashi and H. Tadokoro, *Macromolecules*, **6**, 672 (1973).
21. J. Brandrup and E. H. Immergut (Eds.), "Polymer Handbook", 3rd ed., Willey-Interscience, New York, 1989.
22. J. N. Israelachvili, "Intermolecular and Surface Forces", Academic Press, New York, 1985.
23. F. J. Ansorena, M. J. Fernandez-Berridi, M. J. Barandiaran, G. M. Guzman, and J. J. Iruin, *Polym. Bull.*, **4**, 25 (1981).
24. B. Vincent, P. F. Luckham, and F. A. Waite, *J. Colloid Interface Sci.*, **73**, 508 (1980).
25. S. I. Jeon, J. H. Lee, J. D. Andrade, and P. G. de Gennes, *J. Colloid Interface Sci.*, **142**, 149 (1991).
26. G. Hadziioannou, S. Patel, S. Granick, and M. Tirrell, *J. Am. Chem. Soc.*, **108**, 2869 (1986).
27. S. H. Maron and F. E. Filisko, *J. Macromol. Sci.*, **B6**, 57 (1972).
28. S. H. Maron and F. E. Filisko, *J. Macromol. Sci.*, **B6**, 79 (1972).
29. S. I. Jeon and J. D. Andrate, *J. Colloid Interface Sci.*, **142**, 159 (1991).

Electrical Conductivity of the Solid Solutions X ZrO_2+(1−X) Yb_2O_3; 0.01≤X≤0.09

Byoung Ki Choi, Joon Ho Jang, Seong Han Kim, Hong Seok Kim, Jong Sik Park, Yoo Young Kim, Don Kim, Sung Han Lee, Chul Hyun Yo, and Keu Hong Kim*

Department of Chemistry, Yonsei University, Seoul 120-749. *Received November 4, 1991*

ZrO_2-doped Yb_2O_3 solid solutions containing 1, 3, 5, 7 and 9 mol% ZrO_2 were synthesized from spectroscopically pure Yb_2O_3 and ZrO_2 powders and found to be rare earth *C*-type structure by XRD technique. Electrical conductivities were measured as a function of temperatures from 700 to 1050℃ and oxygen partial pressures from 1×10^{-5} to 2×10^{-1} atm. The electrical conductivities depend simply on temperature and the activation energies are determined to be 1.56-1.68 eV. The oxygen partial pressure dependence of the electrical conductivity shows that the conductivity increases with increasing oxygen partial pressure, indicating *p*-type semiconductor. The P_{O_2} dependence of the system is nearly power of 1/4. It is suggested from the linearity of the temperature dependence of electrical conductivity and only one value of $1/n$ that the solid solutions of the system have single conduction mechanism. From these results, it is concluded that the main defects of the system are negatively doubly charged oxygen interstitial in low ZrO_2 doping level and negatively triply charged cation vacancy in high doping level and the electrical conduction is due to the electronic hole formed by the defect structure.

Introduction

Oxides of the rare-earth elements generally have the rare-earth *C*-type structure when the ratio of the radius of oxygen anion to that of metal cation is between 0.60 to 0.89[1]. And the number of oxygen anions occupied on the lattice sites is six and two of eight lattice oxygen sites become vacancies[2]. Accordingly, the oxides of these rare-earth elements have similar physical properties. It was reported that Sm_2O_3, Gd_2O_3 and other oxides belonging to these rare-earth *C*-type oxides have mixed conduction mechanism that ionic conduction occurs predominantly over electronic conduction[3,4], whereas in the case of Yb_2O_3, there were few experimental data because of thermal instability.

Kang *et al.*[5] reported that above 700℃, pure Yb_2O_3 has the activation energy of from 1.92 to 1.95 eV and shows

the *p*-type semiconducting character, but the ionic conduction in the temperature range less than 700℃. According to the report of Dutta *et al.*,[6] studying d.c. electrical property of thin film, Yb_2O_3 is a *n*-type semiconductor. Using emf method, Tare *et al.*[7] reported that Yb_2O_3 is ionic conductor where the oxygen pressure range is from 10^{-6} to 10 atm at 800℃. Also, Rao *et al.*[8] reported that from the result of a.c. study, it has *p*-type electronic conduction at the oxygen pressure of 150 mmHg, and $1/n$ of the oxygen pressure dependence of electrical conductivity is power of 3/16. Also, they observed that main defect is metal vacancy and the activation energy is 1.61 eV when ionic contribution is about 10% at the temperature ranges of 400 to 900℃. Carpentier *et al.*[9] have reported that it has mixed conduction that both ionic conduction and electronic conduction occur simultaneously at the temperature region of 1423 to 1623 K and the oxygen pressure region of 10^{-12} to 1 atm. And the defects are electron, electronic hole and Frenkel disorder of V_{Yb} and Yb_i.

Hitherto, although many studies have been widely carried out to observe the conduction mechanism and defect structure for pure Yb_2O_3, their results bring an contradiction in many cases. So, in this paper, we are going to reveal the conduction mechanism and defect structure of the ZrO_2-doped Yb_2O_3 solid solution in which ZrO_2 is doped into pure Yb_2O_3.

Experimental

Sample Preparation. Pure Yb_2O_3 (99.99%, Aldrich Chemical Co.) and ZrO_2 (99.99%, Aldrich Chemical Co.) powders were weighed to give ZrO_2-doped Yb_2O_3 solid solutions containing 1, 3, 5, 7 and 9 mol% of ZrO_2. These materials were ground and mixed well on agate mortar for 3 hours and then calcined at 650℃ to remove H_2O and CO_2 adsorbed. These mixtures were made into pellets under a pressure of 8×10^5 Pa. To form solid solution they were sintered for 48 hours at 1250℃ and annealed for 24 hours at 1200℃, then quenched to room temperature. Each pellet analyzed by XRD was made into rectangular form with dimensions of $1.1\times0.6\times0.15$ cm^3. For a four-probe contact, four holes were drilled in a row on face.

Sample Analysis. To examine the formation of solid solutions, X-ray diffractometer (Philips PW 1710, CuKα) equipped with graphite monochromator are employed. DTA and TG (Rigaku PTC-10 AC) measurements were performed to investigate any phase transition and mass change due to the concentration change of defect.

Electrical Conductivity Measurements. The electrical conductivity was measured as a function of temperatures from 700 to 1050℃ and oxygen partial pressures from 1×10^{-5} to 2×10^{-1} atm according to Valdes' four-probe technique[10]. The sample was placed in a quartz cell with Pt/Pt-13% Rh thermocouple. The cell has four Pt probes, the inner two probes were used to measure the potential difference by a Leed & Northrup 7555 K-5 type digital multimeter, and the outer two probes were used to measure the current by a Keitheley 610C digital electrometer.

In order to remove polarization effect, the current through the sample was maintained between 10^{-8} and 10^{-2} A by a rheostat and the potential across the two inner probes was maintained less than 0.8 V. If the distances(S) between each probe are same and the ratio of L/S is more than 2, where L is distance between end probes and sample edge, the conductivity can be calculated by Eq. (1).

$$\sigma=\frac{1}{2\pi S}\cdot\frac{I}{V} \tag{1}$$

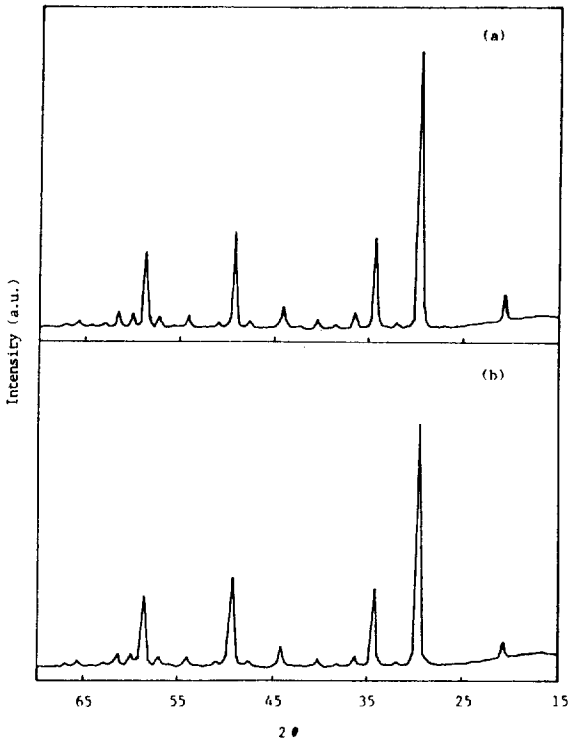

Figure 1. X-ray diffraction patterns of 1(a) and 9 mol% (b) ZrO_2-doped Yb_2O_3 system.

Results and Discussions

Sample Analysis. The results of DTA and TG for 9 mol% ZrO_2-doped Yb_2O_3 imply that in the experimental temperature and oxygen partial pressure regions, no mass change and phase transition occur. So, these samples are thermodynamically stable in experimental region.

X-ray diffraction patterns of 1 and 9 mol% ZrO_2-doped Yb_2O_3 samples are shown in Figure 1. A determination of the *a*-value for each sample was performed using the Nelson-Riley method[11] in order to reduce physical absorption error. The results are shown in Figure 2 and Table 1 for 1 mol% ZrO_2-doped Yb_2O_3 and the lattice parameters(a) of the 1, 3, 5, 7 and 9 mol% ZrO_2-doped Yb_2O_3 samples are plotted against ZrO_2 doping mol% in Figure 3. The lattice parameters of ZrO_2-doped Yb_2O_3 system are linearly decreased as the contents of ZrO_2 increase, which implies that this system forms solid solution with cubic structure. But, this trend is deviated from the pure Yb_2O_3 which has the value of 10.436 Å in ASTM. So, it is expected that the conducting mechanism of pure and ZrO_2-doped Yb_2O_3 systems are different.

Conductivity Results. Figure 4 shows a plot of log σ *vs* 1000/T for the 1 mol% ZrO_2-doped Yb_2O_3 sample in various oxygen partial pressures. As the temperature dependence of conductivity is represented by the equation σ

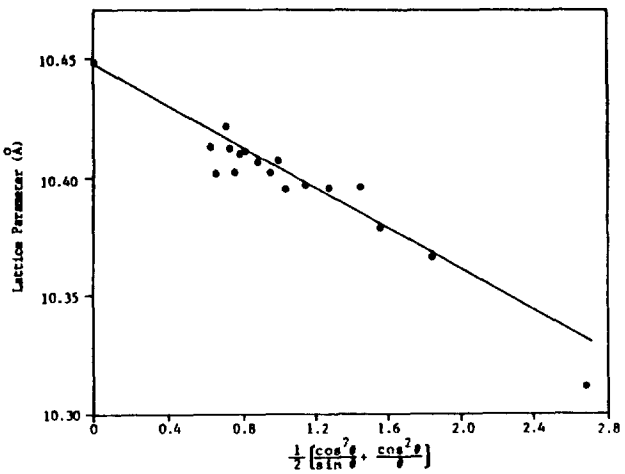

Figure 2. Nelson-Riley plot for 1 mol% ZrO_2-doped Yb_2O_3 sample.

Table 1. Indexation of XRD Diffraction Pattern of 1 mol% ZrO_2-Doped Yb_2O_3

2θ	*h k l*	*F* (θ)	*a*	I/I_0
21.113	2 1 1	2.6834	10.307	9
29.855	2 2 2	1.8435	10.367	100
34.569	4 0 0	1.5607	10.378	31
36.673	4 1 1	1.4566	10.396	6
40.708	3 3 2	1.2852	10.396	4
44.428	4 3 1	1.1528	10.397	8
47.930	5 2 1	1.0453	10.395	4
49.542	4 4 0	1.0005	10.408	27
51.204	4 3 3	0.95692	10.402	3
54.339	6 1 1	0.88125	10.407	4
57.353	5 4 1	0.81545	10.411	5
58.840	6 2 2	0.78519	10.410	25
60.347	6 3 1	0.75586	10.402	6
61.724	4 4 4	0.73016	10.412	6
63.075	5 4 3	0.70591	10.422	3
65.995	7 2 1	0.65646	10.402	1
67.285	6 4 2	0.63581	10.413	1

$=\sigma_o \cdot \exp(-E_a/kT)$, the E_a value for each oxygen partial pressure can be calculated from the slope in a plot of log conductivity against the reciprocals of the absolute temperatures. The results for other mol% ZrO_2-doped Yb_2O_3 samples show the same trend as for 1 mol% in Figure 4, and calculated E_a values under various oxygen pressures are also listed in Table 2.

The dependence of electrical conductivity on oxygen partial pressure for 1 mol% ZrO_2-doped Yb_2O_3 sample is shown in Figure 5 as a plot of log conductivity against log P_{O_2} at various temperatures. The $1/n$ values calculated from the slopes in Figure 5 obtained at various temperatures are about 1/4, and other mol% ZrO_2-doped Yb_2O_3 samples shows the same tendency which are listed in Table 3.

Consideration of Conduction Mechanism. Nonstoichiometric phases have been observed in almost all metal oxides with increase in temperature. So, defect structures

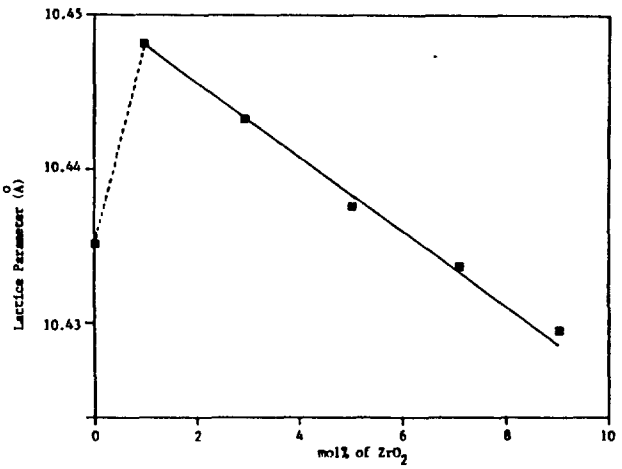

Figure 3. Plot of lattice parameter *vs* doped ZrO_2 mol%.

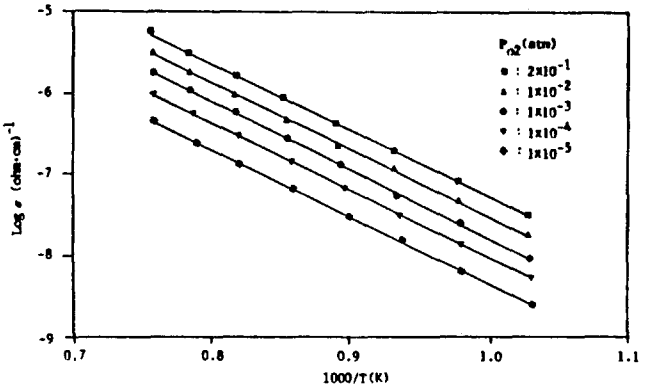

Figure 4. Temperature dependence of electrical conductivity of 1 mol% ZrO_2-doped Yb_2O_3 sample at various oxygen partial pressures.

Table 2. Activation Energies (eV) for Various ZrO_2-Doped Yb_2O_3 System

Doping ZrO_2 mol%	P_{O_2} (atm)				
	2×10^{-1}	1×10^{-2}	1×10^{-3}	1×10^{-4}	1×10^{-5}
1	1.62	1.63	1.67	1.62	1.63
3	1.57	1.59	1.62	1.57	1.63
5	1.63	1.60	1.59	1.58	1.61
7	1.66	1.59	1.64	1.56	1.59
9	1.68	1.62	1.65	1.61	1.64

which can be predicted in this nonstoichiometry can be classified into oxygen deficiency (or metal excess) and metal deficiency (or oxygen excess). The suggested predominant defect in the case of oxygen deficiency are oxygen vacancies or interstitial metal ions and in the case of metal deficiency are metal vacancies or interstitial oxygen atoms. Thus, defects based on thermodynamic data and microscopic techniques are needed to understand the nature of this system and to provide fair interpretations of the conduction phenomena[12]. The conductivities of ZrO_2-doped Yb_2O_3 system are shown in Figure 6. Bacause the slopes of plots for 1, 3, 5, 7 and 9 mol% are nearly the same, samples have the same

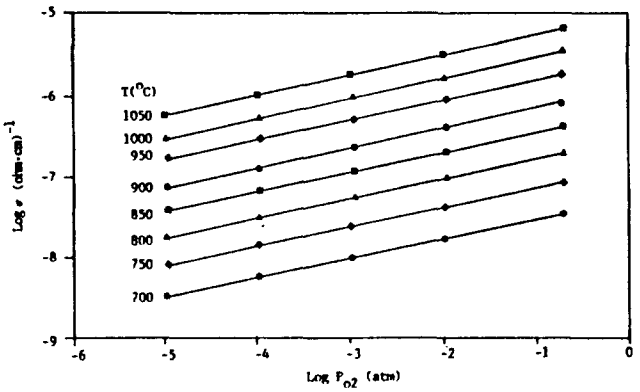

Figure 5. Oxygen partial pressure dependence of electrical conductivity of 1 mol% ZrO_2-doped Yb_2O_3 sample at various temperature.

Table 3. P_{O_2} Dependence (n) of Electrical Conductivity for ZrO_2-Doped Yb_2O_3 System

Doping ZrO_2 mol%	T (℃)							
	700	750	800	850	900	950	1000	1050
1	4.035	3.998	4.009	4.025	4.004	3.963	3.952	3.998
3	4.007	4.039	4.079	3.994	3.984	3.989	4.066	4.004
5	4.032	3.957	3.994	4.025	4.085	3.979	4.055	4.016
7	4.100	4.026	3.963	4.094	3.994	4.104	4.103	3.899
9	4.078	4.087	3.958	4.023	4.008	4.103	4.173	4.043

conductivity properties, but as the amount of doped ZrO_2 increases, the conductivity decreases. From our results for P_{O_2} dependence of electrical conductivities and the reported results[12−15], it is concluded that they are all *p*-type semiconductors and the pure Yb_2O_3 is a metal deficient compound. From the above observation, disorder reactions could be proposed for our samples.

In an intrinsic region, a metal vacancy is formed by the moving of an oxygen atom from the gaseous state into a normal lattice site. The disorder reactions can be expressed as following Kröger notation in which a metal vacancy is ionized and creates electronic holes:

$$3/4 \cdot O_2 \xleftrightarrow{K_1} V_{Yb}''' + 3/2 \cdot O_O + 3 \cdot h^{\bullet} \quad (2)$$

where V_{Yb}''' is negatively triply charged ytterbium vacancy, O_o is lattice oxygen and $h^{\bullet}$ is electron hole. In this case, the equilibrium constant of (2) can be written as follows

$$K_1 = [V_{Yb}'''] \cdot [h^{\bullet}]^3 \cdot P_{O_2}^{-3/4}. \quad (3)$$

If law of mass action is applied to equilibrium (2), at fixed temperature and pressure the concentration of metal vacancy can be represented as

$$1/3 \cdot [V_{Yb}'''] = [h^{\bullet}] = \text{const.} \quad (4)$$

The electrical conductivity dependence on oxygen partial pressure can be represented in terms of electronic hole concentration(p) through Eq. (5)

$$K_1 = 3\ p^4 \cdot P_{O_2}^{-3/4} \quad (5)$$

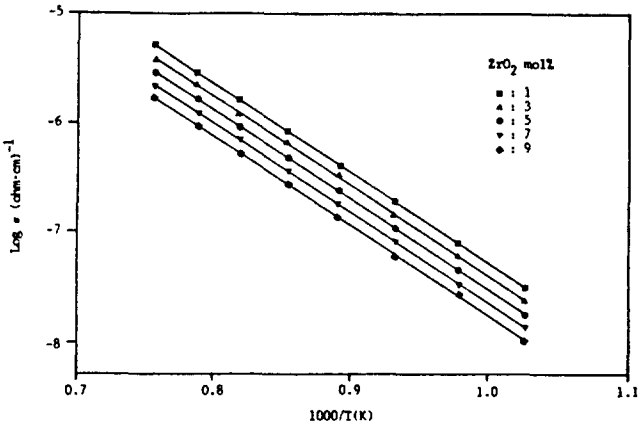

Figure 6. Temperature dependence of electrical conductivity of various ZrO_2-doped Yb_2O_3 samples under 2×10^{-1} atm oxygen partial pressure.

and

$$p = K_1' \cdot P_{O_2}^{3/16} \quad (6)$$

where $K_1' = (K_1/3)^{1/4}$. So, the electrical conductivity dependence on oxygen partial pressure is

$$\sigma \propto P_{O_2}^{1/5.3}. \quad (7)$$

In an extrinsic region which can be influenced by impurities, the mechanism get very complicated. When the doping mol% of ZrO_2 is very low, ZrO_2 reacts with cation vacancies as follows

$$ZrO_2 + V_{Yb}''' \rightleftharpoons Zr_{Yb}^{\bullet} + /2 \cdot O_i'' \quad (8)$$

where $Zr_{Yb}^{\bullet}$ is singly positively charged Zr atom in Yb lattice site and O_i'' is doubly negatively charged interstitial oxygen. Since the conductivity is the sum of intrinsic and extrinsic conduction, equilibria (2) and (8) can be expressed as follows

$$ZrO_2 + 3/4 \cdot O_2 \xrightleftharpoons{K_2} Zr_{Yb}^{\bullet} + 3/2 \cdot O_O + 2 \cdot O_i'' + 3 \cdot h^{\bullet}. \quad (9)$$

For this reaction, the equilibrium constant is

$$K_2 = [Zr_{Yb}^{\bullet}] \cdot [O_i'']^2 \cdot [h^{\bullet}]^3 \cdot P_{O_2}^{-3/4} \quad (10)$$

and the electronic hole concentration is represented as

$$p = K_2'\ P_{O_2}^{1/4} \quad (11)$$

where $K_2' = K_2^{1/3} \cdot [Zr_{Yb}^{\bullet}]^{-1/3} \cdot [O_i'']^{-2/3}$. Therefore, 1 mol% ZrO_2-doped sample has larger lattice parameter than pure Yb_2O_3 due to interstitial oxygen and their conductivities are proportional to $P_{O_2}^{1/4}$.

As the mol% of ZrO_2 doped increases, many interstitial oxygens get thermodynamically unstable and are introduced to lattice sites.

$$3 \cdot O_i'' \rightleftharpoons 3 \cdot O_O + 2 \cdot V_{Yb}''' \quad (12)$$

So, the overall reaction becomes the sum of three times of Eq. (8) and twice of Eq. (12) such that

$$3.ZrO_2 \rightleftharpoons 3 \cdot Zr_{Yb}^{\bullet} + 6 \cdot O_O + V_{Yb}'''. \quad (13)$$

and the disorder reaction which governs the electrical conduction is expressed as follow equation.

$$3\cdot ZrO_2+3/4\cdot O_2 \xrightleftharpoons{K_3} 3\cdot Zr_{Yb}^{\bullet}+2\cdot V_{Yb}^{'''}+15/2\cdot O_O+3\cdot h^{\bullet} \quad (14)$$

In this case, the lattice parameters are decreased because the interstitial oxygen are depleted and the ionic radius of Zr is smaller than that of Yb, which are well fitted with the results of X-ray diffraction. The equilibrium constant of Eq. (14) can be expressed by

$$K_3=[Zr_{Yb}^{\bullet}]^3\cdot[V_{Yb}^{'''}]^2\cdot[h^{\bullet}]^3\cdot P_{O_2}^{-3/4}. \quad (15)$$

Then the electrical conductivity dependence on oxygen partial pressure can be represented in terms of electronic hole concentration

$$p=K_3'\cdot P_{O_2}^{1/4} \quad (16)$$

where $K_3'=K_3^{1/3}\cdot[Zr_{Yb}^{\bullet}]^{-1/3}\cdot[V_{Yb}^{'''}]^{-1/3}$. So, the electrical conductivity dependence on oxygen partial pressure (ι/n) is 1/4. This value agrees well with the experimental value.

From this agreement, we can conclude that the effectively negatively doubly charged oxygen interstitial and the effectively negatively triply charged metal vacancy are predominant in low and high doping level, respectively and that the charge carrier is electronic hole originated from the metal vacancy in Yb_2O_3 system. The fact that the conductivity decreases as the mole fraction of dopant increases as shown in Figure 6 means that metal vacancy formed from equilibrium (14) moves the equilibrium (2) toward left-hand side. Therefore, heavy Zr^{4+} substitution reduces the charge carrier (electronic hole) concentration, so does electrical conductivity.

Acknowledgement. The present studies were support by the Basic Science Research Institute Program, Ministry of Education, Korea, 1990.

References

1. M. Foex and J. P. Traverse, *Rev. Int. Hautes Temper. Refract.*, **3**, 429 (1966).
2. O. T. Sorensen, "*Nonstoichiometric Oxides*", Acadamic press. N. Y., **21** (1981).
3. J. H. Cho. K. H. Chang, K. H. Kim, Y. B. Kim, and J. S. Choi, *J. Kor. Chem. Soc.*, **29**(6), 608 (1985).
4. S. H. Park. Y. Y. Kim, and K. H. Kim. *Bull. Kor. Chem. Soc.*, **11**(4), 339 (1990).
5. Y. H. Kang, J. S. Choi, and K. H. Yoon, *J. Kor. Chem. Soc.*, **18**(1), 23 (1981).
6. C. R. Dutta and K. Barua, *Physica Status Solid(a)*, **71**, KI 81 (1982).
7. V. B. Tare and H. Schmalzried, *Z. Phys chem.*, **43**, 30 (1964).
8. G. V. Subba Rao, S. Ramdas, P. N. Mehrotra, and C. N. Rao, *J. Solid St. Chem.*, **2**, 377 (1970).
9. J. L. Carpentier, A. Lebrun, F. Perdu, and P. Tellier, *J. Phys. Chem. Solids*, **43**(10), 1003 (1982).
10. L. B. Valdes. *Proc. IRE.*, **42**, 420 (1954).
11. J. B. Nelson and D. P. Riley. *Proc. Phys. Soc. London*, **57**, 160 (1945).
12. P. Kofstad, "*Nonsoichiometry, Diffusion and Electrical Conductivity in Binary Metal Oxides*", John Wiley & Sons Inc., N. Y., 1972, p. 6.
13. W. Noddack and H. Walch, *Z. Elecktrochem.*, **63**, 269 (1959).
14. G. V. Subba Rao, S. Ramdas, P. N. Mehrotra, and C. N. Rao, *J. Solid State Chem.*, **2**, 377 (1970).
15. Y. Wilbert, N. Dherbomez, and H. Breuil, *Compt. Rend. Ser. C.*, **280**, 465 (1975).

Syntheses and Phase-transfer Catalytic Activities of Monoazacrown Ethers

Jae Hu Shim*, Kwang Bo Chung, and Masao Tomoi†

Department of Chemical Engineering, Dongguk University, Seoul 100-715
†Department of Applied Chemistry, Faculty of Engineering, Yokohama National University, Yokohama 240, Japan. *Received January 3, 1992*

Preparative methods for and catalytic activities of monoaza-18-crown-6 or monoaza-15-crown-5 in the reaction of 1-bromooctane with aqueous KI or NaI were investigated. Monoazacrown ethers were prepared by debenzylation of N-benzylmonoazacrown ethers, obtained from the reaction of N-benzyldiethanolamine and oligoethylene glycol ditosylate. The phase-transfer catalytic activity of N-benzylmonoazacrown ethers was higher than that of the corresponding monoazacrown ethers.

Introduction

Since pioneering works by Pedersen[1] a large variety of macrocyclic compounds have been prepared and their cation complexation properties have been investigated extensively[2]. The aza-crows have complexation properties that are intermediate between those of the all-oxygen crowns, which strongly complex alkali and alkaline earth matal ions, and